4.2.7 Muon Detection

The BTeV muon system has two primary functions:

- J/ψ and Prompt Muon Trigger: Besides providing interesting physics, this trigger performs an important service role by selecting (bottom) events on which the more aggressive and technically challenging triggers (such as the vertex trigger) can be debugged and evaluated.
- Muon Identification: Many of the experiment's physics goals (rare decay searches, CP violation studies which require tagging, studies of beauty mixing, searches for charm mixing, etc.) rely on efficient muon identification with excellent background rejection.

We have selected a magnetic (toroidal) design combined with fine-grained tracking elements (described in detail in a subsequent chapter). This design permits "stand-alone" momentum/mass triggering: *i.e.* a muon trigger based solely on information from the muon detector. In addition, improved background rejection is possible via comparisons of this stand-alone measurement with momentum and tracking information from the rest of the spectrometer. The design of the system, including the fine-grained detector segmentation, has been chosen to reduce and uniformly distribute occupancies and to minimize confusion in pattern recognition (both at the trigger level and in offline reconstruction).

In order to provide a viable trigger, the system must get a rejection at Level 1 of a few 10^{-2}. The goal for muon misidentification is 10^{-3}.

Given the objective of a "stand-alone" trigger and the size limitations set by the experimental hall, one can make fairly general calculations that place specific (and restrictive) constraints on the design of the system. We will first describe these general calculations and use them to motivate the overall design of the muon system. We will then describe trigger efficiency and rejection studies we have performed for $B^0 \to J/\psi K^0_s$, which illustrate the performance of the design for a specific (and important) physics mode.

4.2.7.1 General Design Considerations

In the absence of any special momentum dependent coordinate weighting designed to reduce the effects of multiple Coulomb scattering, the fractional momentum resolution in a magnetic spectrometer can be parameterized by the expression:

$$\frac{\sigma_p}{p} = \sqrt{a^2 + (b\ p)^2} \tag{4.12}$$

In Equation 4.12, the a term depends on the bending power and multiple scattering environment of the detectors, while the b term depends on the bending power and and the detector layout and spatial resolution. Fig.4.41 shows that the potential rejection provided by a trigger for low momentum muons significantly degrades once the low momentum fractional resolution exceeds 25%. An $a = 25\%$ value means that the trigger rejects very soft muons at roughly the 4σ level. At higher momentum, where multiple scattering is less important,

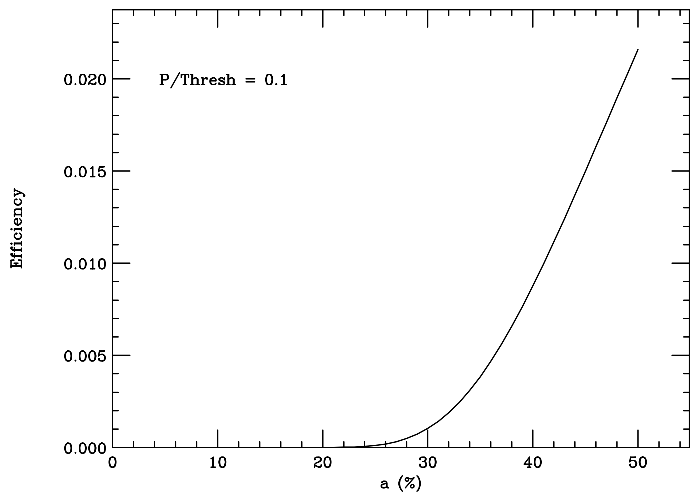

Figure 4.41: The efficiency, calculated in a simple Gaussian model, for a muon with 1/10 the threshold momentum to pass a momentum threshold as a function of a, the MCS term in the resolution formula. We say that a muon at the threshold momentum should fire the trigger 50% of the time. Note the dramatic rise in sensitivity above $a = 25\%$.

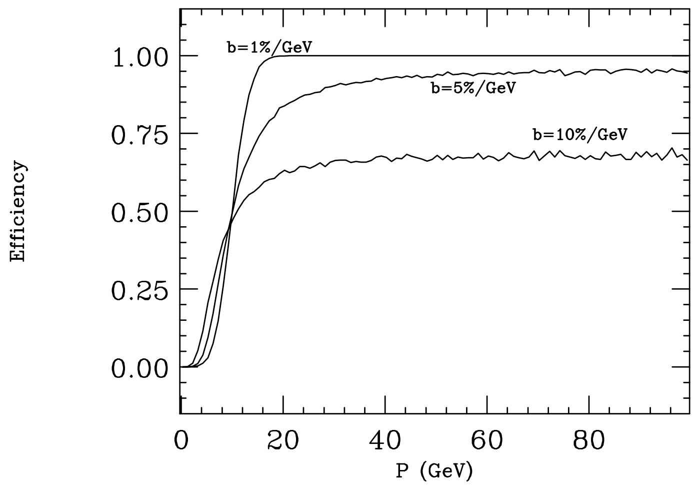

Figure 4.42: Simulated trigger efficiency as a function of muon momentum for a trigger designed to fire with a 50% efficiency at 10 GeV. The multiple scattering dominated term is set to $a = 25\%$ while the measurement dominated term varies from $1\%/GeV < b < 10\%/GeV$.

one becomes sensitive to the b term of Eq. 4.12. The high momentum resolution influences how sharp a momentum threshold one can make in a stand-alone muon trigger. Figure 4.42 illustrates this point by showing the trigger efficiency as a function of momentum for several b values.

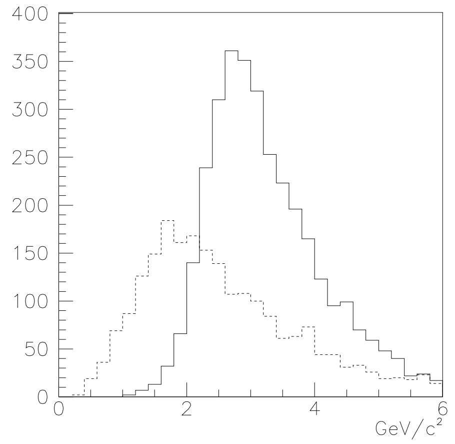

Figure 4.43: Reconstructed $J/\psi \to \mu^+\mu^-$ mass resolution for $b = 1\%/GeV$ (solid) and $b = 5\%/GeV$ (dashed), where b is defined in Eq. 4.12. Equal numbers of J/ψ candidates were generated for each case.

These considerations suggest minimum performance criteria of $a < 25\%$ and $b \leq 1\%/GeV$. As a further illustration, Fig. 4.43 shows the mass resolution obtainable at the trigger level for $J/\psi \to \mu^+\mu^-$ events for two values of b.

4.2.7.2 Possible Design Layouts

Several possible measurement and shielding layouts were studied before we reached the baseline design. In assessing possible layouts, we compute the momentum resolution using an error matrix which incorporates Gaussian models for both the detector resolution and multiple Coulomb scattering. The beam is modeled as a Gaussian beam spot with $\sigma_x = \sigma_y = 1$ mm and $\sigma_z = 30$ cm. In cases where there is redundant coordinate information, the error matrix assumes that the fit weighted the space points according to momentum in order to get the best possible momentum measurement.

Our early calculations showed that it is not possible to get a good momentum measurement using just the dispersion provided by the central dipole (and a constraint that muon system tracks point back to the interaction point). The extrapolation distance is too large given the level of multiple scattering up to the muon planes, making it infeasible to point the muon track segment back to the interaction region. A magnetic toroid with magnetic fields circulating in the $\hat{\phi}$ direction is the only (simple) option which allows us to trigger effectively using tracking information from only the muon system.

The first arrangement we considered is illustrated in Figure 4.44. In this design, one determines the momentum of a muon by measuring its slope in $\hat{\theta}$ before and after a toroid. The entering and exiting slopes of the muon are measured using two pairs of measuring stations (μ_1–μ_4) separated by one meter lever arms. At low momentum, where the multiple scattering dominates resolution, a single 1.5 Tesla, 1 meter thick toroid achieves the required

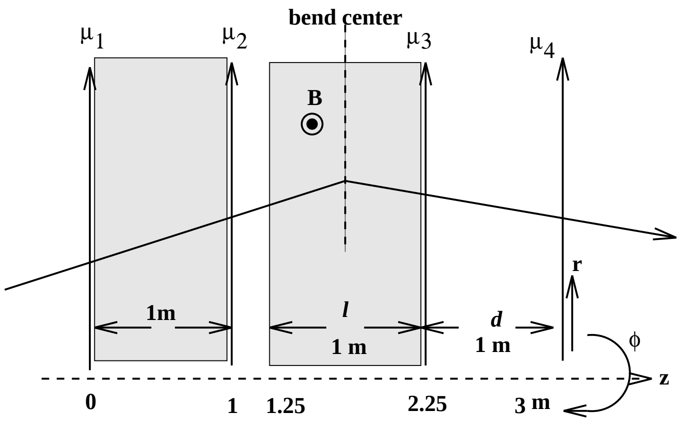

Figure 4.44: Layout of one arm of the muon detector in $2 \oplus 2$ geometry.

fractional momentum resolution of $a = 25\%$. In this arrangement the steel between the measurement stations of the upstream doublet (μ_1–μ_2) primarily serves to shield the muon system from hadrons and need not be magnetized. The requirement of good momentum resolution ($b \approx 1\%/GeV$) dictates a spatial resolution of $\sigma = 2.5$ mm. We will call this the "$2 \oplus 2$" geometry.

Note that the intrinsic rms spatial resolution ($\sigma = 2.5$ mm) required by this (and subsequent) geometries is consistent with what we require from timing considerations alone. Timing information is useful for rejecting background hits such as those associated with accelerator backgrounds (these hits come 60–70 ns before tracks from the interaction point). Assuming a fast gas drift velocity of roughly 9 cm/μs, a drift tube system with a maximum drift time of 30 ns has a maximum drift length of 2.5 mm (leaving 30 ns for charge integration). For a double layer of 1 cm diameter round proportional tubes, offset by half a tube in a "picket fence" design (to avoid dead regions between the tubes), the maximum drift time for the first signal from a track is 30 ns. This arrangement yields an rms resolution of $\sigma = 1.44$ mm.

The major problem with the $2 \oplus 2$ design is that the most upstream of the four detector stations is unshielded against hadronic showers originating in the electromagnetic calorimeter and is thus likely to be too confused for use in a first level trigger. One could, in principle, measure momentum using the downstream doublet μ_3 and μ_4 and a single upstream point μ_2. This geometry gives essentially the same a parameter, but for the same spatial resolution the b parameter is degraded by a factor of 2.8 because the effective upstream lever arm has been reduced to just the distance between the bend center and μ_2.

This led us to the revised design, our "baseline" geometry, illustrated in Fig. 4.45 where the upstream muon trajectory is measured using information from the nominal beam constraint. The effectiveness of this approach is illustrated in Fig. 4.46. The upper black curves give the fractional momentum resolution as a function of muon momentum for the case where only the downstream steel is magnetized and only information from μ_3, μ_4 and the nominal beam center is used. The three curves are for muons emerging at three different azimuthal

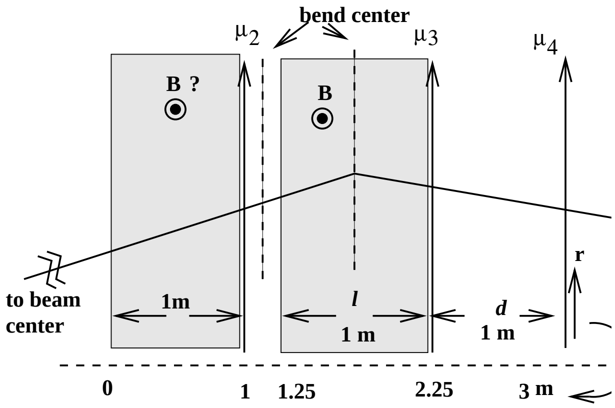

Figure 4.45: Layout showing the baseline geometry. The downstream trajectory is measured by μ_3 and μ_4. The upstream trajectory is measured using the nominal beam center with possible help from μ_2. In order to get sufficient bending power, both steel sections will need to be magnetized.

(ϕ) angles. The pronounced azimuthal variation in fractional momentum resolution arises because of constructive and destructive interference between the dipole and toroid fields. Figure 4.46 shows that at destructive ϕ angles, the a term exceeds our criteria of $a < 25\%$.

The incorporation of information from μ_2 significantly helps the fractional momentum resolution for the case of a single toroid at low momenta as shown in the three blue curves of Fig. 4.46. Essentially the fit used to obtain the "blue" resolution curves ignores the beam constraint at low momentum while exploiting it at high momentum through momentum varying weights. Such a resolution is obtainable off-line, but would be difficult to achieve in a first level trigger.

If one instead magnetizes both the upstream and downstream steel, the bending power of the toroid overwhelms the power of the dipole and a much simpler triggering scenario emerges which is illustrated by the lower seven curves of Fig. 4.46. The case where only a beam constraint and μ_3–μ_4 are used in the trigger is illustrated by the dashed red curves. The green curve shows the resolution one would obtain using a beam constraint and the downstream μ_3-μ_4 doublet if the central dipole were turned off. The green curve shows that the dipole provides very little additional bending power in the ultimate system. When information from μ_2 is included one gets the solid magenta curves. Again, curves are shown for three different azimuths. Each of these curves exhibit good performance relative to our criteria on a and b (over the complete azimuth).

Interestingly enough, Fig. 4.46 tells us that in a two magnet, toroid geometry, μ_2 contributes very little to the momentum resolution. In the absence of noise or confusion, one can design a very simple but effective trigger by correlating information from just the two $\hat{\theta}$ views of the downstream doublet consisting of μ_3 and μ_4 and the nominal beam center. Since this is the minimal amount of information required to obtain a momentum estimate, no momentum dependent weighting of detector information is used. We also have the benefit of deriving this trigger from the most shielded chambers of the muon system, minimizing

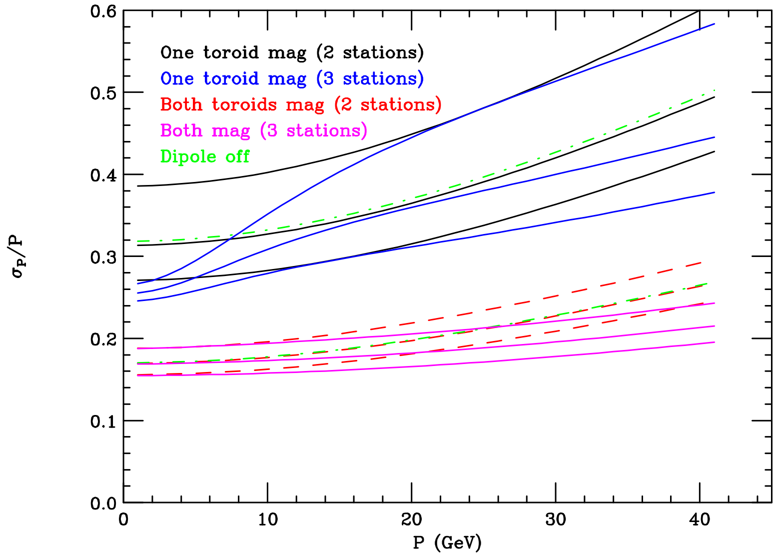

Figure 4.46: Plots of the fractional momentum resolution as a function of momentum for various readout scenario's of the BTeV muon system. All plots assume chambers with 2.5 mm rms spatial resolution. The plots appear in groups of 3 corresponding to $\phi = 270^o$ (best) 0^o and 90^o (worst). The ϕ dependence of the resolution illustrates interference between the central dipole and muon toroid(s). The black and red families of curves illustrate the case where only the two stations after the second toroid are used in the trigger. In this case the trajectory upstream of the toroid comes entirely from the beam constraint. The blue and magenta curves illustrate the case where the station between the two toroids is used to help determine the trajectory prior to the toroids. The green curves assume only the final two stations are used, and that the dipole is turned off .

hadronic punch-through effects.

Although μ_2 is not required to measure muon information in our two toroid scenario, it is likely to be of substantial use in eliminating false triggers due to noise and confusion. Figure 4.47 illustrates just one example by showing how μ_2 can be used at the trigger level to eliminate false triggers from soft muons with an accompanying δ-ray.

4.2.7.3 Baseline Design

Based on the above, our baseline muon system consists of two 1 m thick iron toroids and three measurement stations with spatial resolutions of $\sigma = 1.5$ mm. Each of the measurement stations is separated by approximately 1 meter. The spatial resolution is set by both timing considerations and momentum resolution requirements.

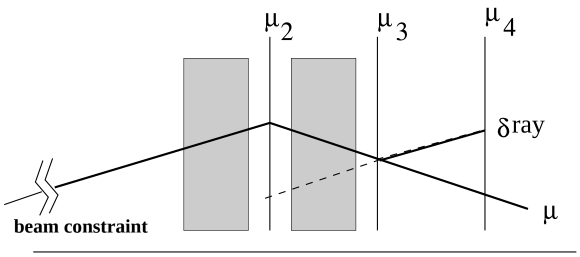

Figure 4.47: This figure illustrates the usefulness of μ_2 in reducing false triggers due to confusion from δ-rays. We illustrate a trajectory for a low momentum μ which is severely bent by the two toroids and therefore extrapolates far from the nominal beam center. As this muon emerges from μ_3 it emits a wide angle δ-ray which leaves an additional hit in μ_4. In the case illustrated, the two hits in stations μ_3 and μ_4 from the δ-ray point back to the nominal beam center and mimic a high momentum muon. However, the δ-ray trajectory extrapolates very far from the muons hit in μ_2 and thus fails to satisfy a trigger which requires a confirming hit in μ_2.

4.2.7.4 Trigger Studies for $B^0 \to J/\psi K_s^0$

We have studied the triggering performance of our baseline muon system using MCFAST. We used minimum bias events to study rejection ratios and $B^0 \to J/\psi\, K_s^0$, where $J/\psi \to \mu\mu$, to investigate trigger efficiency. The minimum bias events were generated with Pythia and include elastic scattering, single and double diffractive, low p_T scattering and semi-hard QCD $2 \to 2$ processes. Events are overlapped to simulate multiple events per crossing. The number of events per crossing is generated from a Poisson distribution with average two. In generating the $B^0 \to J/\psi\, K_s^0$ events, minimum bias events are also added so that the total number of interactions per crossing is also Poisson with an average of two. For the studies presented below, we only consider "real" muons, which can be prompt or can come from decays in flight. In minimum bias events, the muons come almost entirely from pion (70%) and kaon (30%) decays. "Fake" muons from punch through, delta rays, and noise hits in the chamber are not yet simulated.

In the calculations below, efficiency is the ratio of accepted events to generated events. This includes geometrical acceptance and the selection cuts. For our purposes, a signal ($B^0 \to J/\psi\, K_s^0$) event is considered to be in the geometrical acceptance if both tracks from the J/ψ muons are tracked by the silicon and make it through all stations of the muon system. The muon system is assumed to have an outer radius of 2.4 m and the inner radius is varied between 10 cm and 20 cm (10 cm is the smallest possible inner radius given the inner radius of the toroids, while 15–20 cm is the smallest inner radius that can probably be achieved with the baseline design). At that point, both minimum bias and signal events are treated identically. They are accepted if muon(s) in the event pass cuts on momentum, transverse momentum, and/or a minimum invariant mass cut on muon pairs. In all cases where two muons are required, they must have opposite sign and be in different octants in ϕ (each detector plane in the baseline muon system is divided into eight pie shaped octants).

The pair of muons must also be in the same arm of the detector.

The momentum and transverse momentum of each muon in the event is obtained by smearing its generated momentum using the appropriate resolution (see Fig. 4.46) and smearing function. We then vary the cuts on momentum, transverse momentum, and invariant mass of pairs of muons and make two dimensional plots showing rejection of minimum bias events on one axis and J/ψ efficiency on the other. An example plot is shown in Fig. 4.48. We have made similar plots for differing inner radii, one versus two toroids, and so on. Based

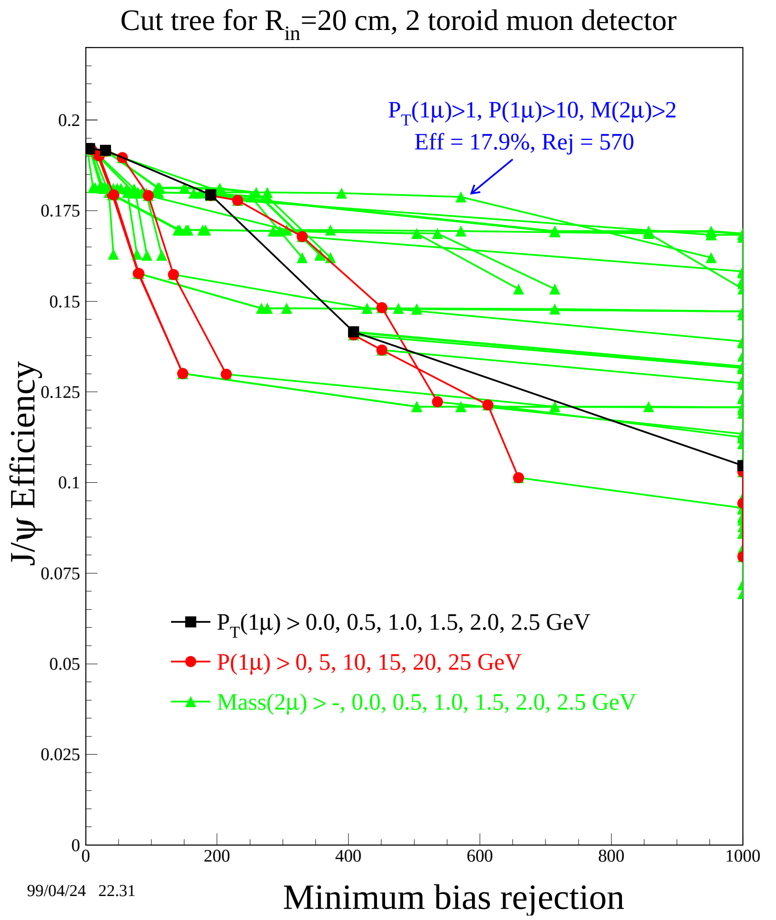

Figure 4.48: Absolute J/ψ efficiency versus minimum bias rejection for cuts on the minimum muon p_T, the minimum muon momentum and the minimum invariant mass. Black lines connect the squares which show the variation as the minimum muon p_T is increased. From each black square a red line connecting the circles shows the change as the minimum muon momentum is increased. From each red circle a green line connecting the triangles shows the variation as the minimum invariant mass requirement is increased. A cut of "-" indicates no cut. Results are for a two-toroid muon detector with inner radius of 20 cm.

on these studies, we find typical rejection ratios of 500-600 with efficiencies of roughly 18%. Note that the geometric acceptance (no momentum or mass cuts) of a 10 cm inner radius system is 22%. Based on these studies, we have found:

1. Most of the rejection power comes from requiring minimum p and p_T for two muons in the event. An invariant mass cut is beneficial, but is not required to obtain large rejections with good efficiency. If it turns out that an invariant mass cut is difficult to implement in the first level trigger, we will not be at a severe disadvantage.

2. An inner radius of 15–20 cm is acceptable. If we insist on a rejection ratio of 500 or more, the efficiency for signal events is 18.8% for an inner radius of 10 cm and 17.9% for an inner radius of 20 cm (20 cm is worst case).

3. Two toroids are needed. If we require a rejection ratio of 500–600, the efficiency for signal events drops significantly (from ∼18% to ∼14%) in going from two toroids to one. In fact, it appears that the only hope for a single muon trigger is the two toroid case: acceptable rejections are not possible with only one toroid.

4.2.7.5 Summary of Detector Requirements

To summarize, the BTeV muon system should have the following attributes:

1. Robust: It will be very difficult to access the detectors once they are installed.

2. High Rate Capability: Rates of a few kHz/cm^2 are possible in parts of the system (based on calculations of accelerator backgrounds).

3. Good Time Resolution: Timing information on hits with a resolution of 50–60 ns will allow rejection of hits due to accelerator backgrounds.

4. Magnetic: Two toroids of 1.5 Tesla field and roughly 1 m thickness (in each arm).

5. Fine-Grained Spatial Resolution: Tracking resolutions of 2–3 mm are required.

6. Longitudinal Compactness: Given the size constraints, the detectors should be of minimal thickness.

7. Minimal Neutron Susceptibility: We will avoid the use of hydrogenic detector elements.

8. Uniform Occupancy: A geometry designed to minimize pattern recognition confusion and minimize occupancy at smaller radii.

The details of the baseline muon system design are discussed in a subsequent chapter.